Giant electron-phonon interaction for a prototypical semiconductor interface: Sn/Ge(111)-(3 × 3)

M. N. Nair [1,2,*], I. Palacio [2,*], A. Mascaraque [3,4], E. G. Michel [5,6], A. Taleb-Ibrahimi [2],
A. Tejeda [1,2], C. González [3,4], A. Martín-Rodero [7,6], J. Ortega [7,6], and F. Flores [7,6]

[1]*CNRS, Université Paris-Saclay, Laboratoire de Physique des Solides, F-91405 Orsay, France*

[2]*Synchrotron SOLEIL, L'Orme des Merisiers, Saint-Aubin, F-91192 Gif sur Yvette, France*

[3]*Departamento de Física de Materiales, Universidad Complutense de Madrid, E-28040 Madrid, Spain*

[4]*Instituto de Magnetismo Aplicado UCM-ADIF, E-28230 Madrid, Spain*

[5]*Departamento de Física de la Materia Condensada, Facultad de Ciencias, Universidad Autónoma de Madrid, E-28049 Madrid, Spain*

[6]*Condensed Matter Physics Center (IFIMAC), Universidad Autónoma de Madrid, E-28049 Madrid, Spain*

[7]*Departamento de Física Teórica de la Materia Condensada, Facultad de Ciencias,
Universidad Autónoma de Madrid, E-28049 Madrid, Spain*

We report an experimental and theoretical study of the electron-phonon coupling for α-Sn/Ge(111), a prototypical triangular lattice surface, closely related to Sn/Si(111)-($\sqrt{3} \times \sqrt{3}$), where recent experimental evidence has found superconductivity [X. Wu *et al.*, Phys. Rev. Lett. **125**, 117001 (2020)]. We concentrate our study on the (3 × 3) phase of α-Sn/Ge(111) that appears between 150 and 120 K and has a well-known geometry with a half-filled electronic band around the Fermi energy. We show that this surface presents a giant electron-phonon interaction that can be considered at least partially responsible for the different phases that this system shows at very low temperature. Our theoretical results indicate that indeed the electron-phonon interaction in α-Sn/Ge(111)-(3 × 3) is unusually large, since we find that λ, the electron mass enhancement for the half-filled band, is $\lambda = 1.3$. This result is in good agreement with the experimental value obtained from high-resolution angle-resolved photoemission spectroscopy measurements, which yield $\lambda = 1.45 \pm 0.1$.

I. INTRODUCTION

Low-dimensional solids have been widely studied during the last years due to their exotic properties [1]. Surfaces are a prominent example, since the reduction of dimensionality from three dimensions (3D) to two dimensions (2D) enhances the importance of fluctuations and entropic effects as well as the role played by electronic correlations in surface states in competition with the degree of coupling between those surface states and the lattice phonons. The variety of surface phenomena encompasses Mott phases, charge density waves, Thouless-Kosterlitz phases, magnetism, and superconductivity [1–13].

The α-Sn/Si(111) and α-Sn/Ge(111) surfaces, obtained by covering a Si or Ge substrate with 0.33 monolayers (ML) of Sn, have been widely studied due to their interesting and complex physical behavior. Recently, Weitering *et al.* [2] have observed superconductivity associated with the Sn/Si(111)-($\sqrt{3} \times \sqrt{3}$)$R30°$ surface states. On the other hand, calculations made for K/Si(111):B-($\sqrt{3} \times \sqrt{3}$)$R30°$ [14] suggest that for Si-dangling bonds the strength of the electron-phonon (*e*-ph) interaction is very similar to the electron-electron (*e*-*e*) repulsion, indicating that also in α-Sn/Si(111) there might be a close competition between the repulsive *e*-*e* and attractive *e*-ph interactions [2,15]. An impor-

tant *e*-ph interaction associated with partially occupied surface bands has also been observed in Si(111)-(7 × 7) ($\lambda = 1.06$ [16]) and in Ge/Si-(5 × 5) ($\lambda \simeq 0.53$ [17]). Electron-phonon coupling is thus an important element to accurately describe semiconducting surfaces with metallic two-dimensional surface states, and to understand a possible superconductor state and other phase transitions [2,15,18,19].

In this paper we analyze the (3 × 3) phase appearing between 150 and 120 K [4,6] at the α-Sn/Ge(111) paradigmatic surface with a combined experimental and theoretical approach to elucidate the importance of the *e*-ph coupling, poorly studied in the past. The (3 × 3) phase has a well-known structure that allows us to perform an accurate analysis of its *e*-ph properties. Our theoretical results indicate that in this surface the *e*-ph interaction is unusually large, $\lambda = 1.3$, in good agreement with the value of $\lambda = 1.45$ found by angle-resolved photoemission spectroscopy (ARPES) experiments. We conclude that the strengths of the *e*-ph and *e*-*e* interactions are comparable, indicating that the *e*-ph interaction should play an important role in the stabilization of the low-temperature phases of α-Sn/Ge(111) [4].

II. ELECTRONIC SURFACE BANDS AND PHONONS

Sn atoms occupy T_4 sites of the Ge(111) substrate in the Sn/Ge(111)-(3 × 3) reconstruction, which is characterized by a vertical distortion, so that one of the three Sn atoms in the unit cell is at a higher position than the other two [see
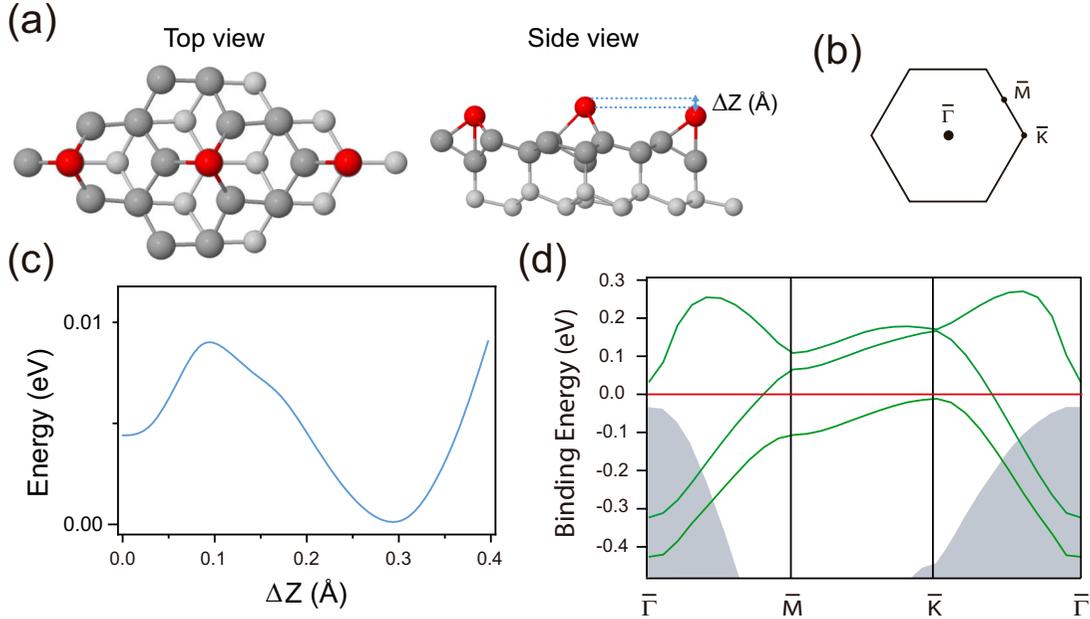
FIG. 1. (a) Top and side views of the Sn/Ge(111)-(3×3) surface. (b) Surface Brillouin zone. (c) Energy per (3×3) unit cell associated with the (3×3) distortion; $\Delta Z = (\Delta z_{up} - \Delta z_{down})$, where Δz_{up} and Δz_{down} are the vertical displacements of the up and down Sn atoms. (d) DFT surface bands; the shaded areas represent the projection of the bulk bands and the red line at 0 eV indicates the Fermi energy E_F.

Fig. 1(a)]. The interface presents three surface bands. One of them is completely filled and is related to the dangling bond state of the Sn atom moving up. The dangling bond states of the two Sn down atoms create the two other surface states; a bonding combination of those dangling bonds is associated with the metallic band crossing the Fermi energy [7,20]. Figure 1(d) shows the three surface bands as calculated with density functional theory (DFT) [21] while the bands below the Fermi energy measured with ARPES are shown in Fig. 2(a). Notice that the theoretical bandwidth of the metallic band below E_F is around 0.3 eV, while the experimental width of this band is around 0.2 eV. This is probably due to the *e-e* interaction which, as discussed in the Supplemental Material (SM) [21] (see also Refs. [22,23] therein), yields a band narrowing effect of around 1/1.6, close to the experimental value.

We are interested in calculating the *e*-ph coupling associated with the active half-occupied band and the surface phonons of the Sn/Ge(111)-(3×3) surface, assuming that the active band has the measured photoemission bandwidth. As discussed in Ref. [24], we find three different phonon surface modes associated with the following displacements of the three Sn atoms of the (3×3) unit cell along the direction (z) perpendicular to the surface: $\vec{u}_1 = (1, 1, 1)/\sqrt{3}$, $\vec{u}_2 = (1, -1, 0)/\sqrt{2}$, and $\vec{u}_3 = (-1, -1, 2)/\sqrt{6}$. The first mode, $\vec{u}_1$, only introduces a rigid displacement of the three electron surface bands. The second mode, $\vec{u}_2$, interacts weakly with the bonding state of the half-occupied band due to its symmetry. The crucial mode interacting with the active band is $\vec{u}_3$, which introduces the same distortion appearing at the (3×3) phase (see below).

Figure 1(c) shows the energy per (3×3) unit cell along the distortion path defined by the trajectory $(\sqrt{3} \times \sqrt{3})R30° \rightarrow (3 \times 3)$, where the $(\sqrt{3} \times \sqrt{3})R30°$ corresponds to a flat

structure with equivalent Sn atoms, as calculated using DFT techniques [21]. The down atoms move to a very good approximation with 1/2 of the displacement associated with the up atom, $\Delta z_{down} \simeq -0.5\Delta z_{up}$ [25]. As expected, the energy minimum appears for the (3×3) structure with ~ 5 meV lower energy [4,20,25,26] than the $(\sqrt{3} \times \sqrt{3})R30°$ structure, and for a relative displacement, $\Delta Z_0 = \Delta z_{up} - \Delta z_{down}$, of 0.29 Å [7,20]. The $\vec{u}_3$ phonon mode is associated with the potential around that minimum. Calculations and He-scattering experiments [24] indicate that the corresponding phonon energy, ω_0, is around 4.3 meV. From our DFT calculations [Fig. 1(c)], we obtain the potential $V \approx 1/2K\eta^2$ around $\eta = 0$ ($K = 0.70$ eV/Å^2), where $\vec{\eta} = \eta(-1, -1, 2)/\sqrt{6}$ defines the normal mode along the $\vec{u}_3$ direction. As $\omega_0 = \sqrt{K/M}$, we can also calculate $M = 172m_p$ (m_p is the proton mass), in good agreement with Ref. [25].

III. PHOTOEMISSION EXPERIMENTS AND SURFACE BANDS

The fluctuating $(\sqrt{3} \times \sqrt{3})R30°$ reconstruction observed at room temperature freezes into the (3×3) metallic phase shown in Fig. 1 below 150 K. A sharp (3×3) low-energy electron diffraction (LEED) pattern is observed in the 150–120 K range. Below this temperature, however, the intensity of the (3×3) spots weakens [4]. The *e*-ph interaction can be analyzed experimentally by looking at the mass enhancement effect that this interaction introduces in a metallic band around the Fermi energy. This can be accurately determined by means of ARPES measurements [27–30].

We have explored with ARPES the electron mass enhancement associated with the *e*-ph interaction in the 120–150 K temperature range. Figure 2(a) shows the second derivative of the ARPES data along the $\overline{\Gamma M}_{3 \times 3}$ direction, where $\overline{\Gamma}$
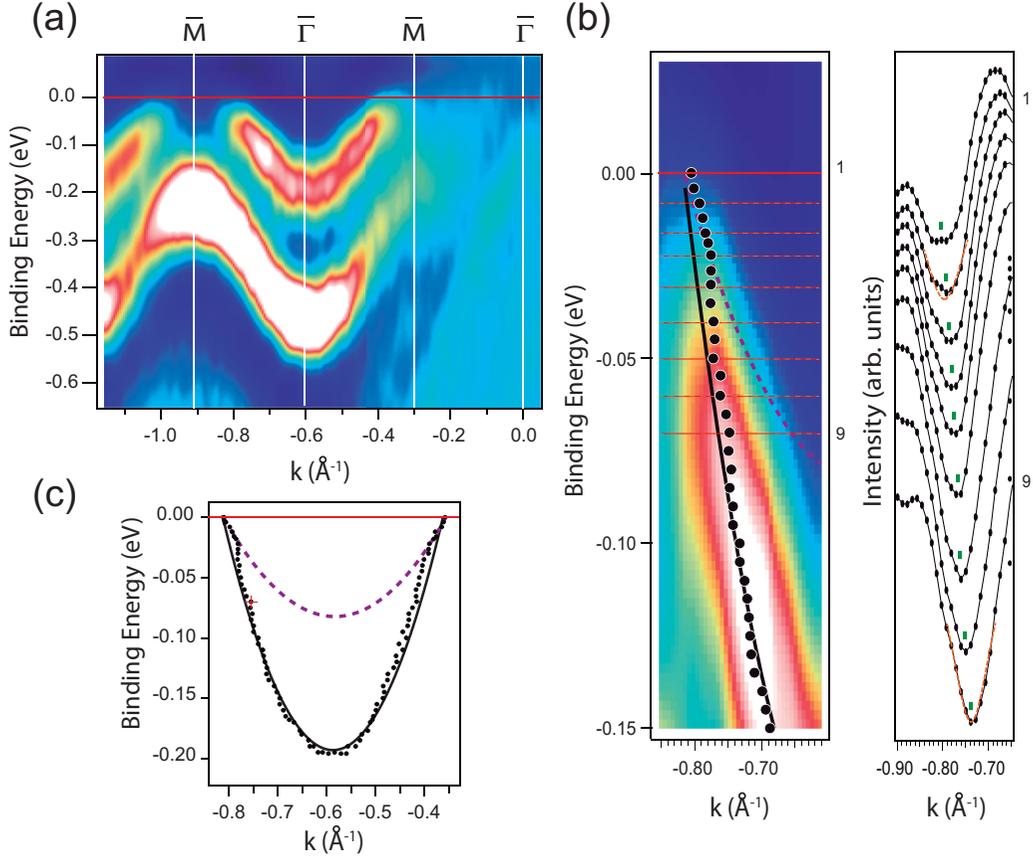
FIG. 2. (a) Second derivative of the ARPES data along the $\overline{\Gamma M}_{3\times3}$ direction in the second BZ (see text). (b) Left panel: Fermi level region from (a). Right panel: Momentum distribution curves corresponding to the red lines shown in the left panel. Note that the momentum distribution curves exhibit minima at the location of the band because the figure shows the second derivative of the data. The minima (green tick marks) are fit to Lorentzians (red lines, two fits are shown). The corresponding points appear in the left panel. (c) Experimental points and fit to the bare (black line) and the renormalized (dashed purple line) bands, also shown in (b) (left).

belongs to the second Brillouin zone (BZ). The surface presents two bands, one completely filled band associated with the up atoms and a metallic band related to the down atoms. The detail of the region of the metallic band closer to the Fermi level [Fig. 2(b)] shows that the electronic band does not follow the parabolic dispersion of the band at higher binding energies characterized by the bare effective mass m_0. The spectral weight in the two branches of the parabola centered around -0.6 Å^{-1} is not equivalent, as often happens in photoemission, due to matrix element effects [31]. Close to the Fermi level, a kink develops in the metallic band, the slope of the band decreases, and the effective mass is affected by the e-ph coupling in such a way that $m^* = (1 + \lambda)m_0$. λ can be obtained from the experimental values of m_0 and m^* with no further assumption. We have therefore determined the band dispersion [dots in Figs. 2(b) and 2(c)] from a fit of the momentum distribution curves to Lorentzian peaks. Once the experimental dispersion was accurately determined, the data were fitted to two parabolas in order to extract m_0 and m^*. Figure 2(c) shows that the renormalized parabola fits both branches of experimental data, thus providing great confidence in the determination. A perfect agreement is, however, not expected since the state does not follow an ideal parabolic dispersion in the considered energy range, as evident from the theoretical bands [Fig. 1(d)]. From these fittings,

the e-ph mass enhancement parameter is determined to be $\lambda = 1.45 \pm 0.1$, a very large value when compared to the usual values of λ in other surfaces [32].

IV. ELECTRON-PHONON INTERACTION: CALCULATION OF g AND λ

We analyze theoretically the e-ph interaction by means of the following Holstein Hamiltonian [33],

$$\hat{H} = \sum_{i\sigma} \epsilon_0 \hat{n}_{i\sigma} + \sum_{ij\sigma} T_{ij} \hat{c}_{j\sigma}^+ \hat{c}_{i\sigma} + \sum_i \omega_0 \hat{b}_i^+ \hat{b}_i$$
$$+ \sum_i g(\hat{b}_i^+ + \hat{b}_i)(\hat{n}_{i\uparrow} + \hat{n}_{i\downarrow} - 1), \qquad (1)$$

where a local i phonon, the $\bar{u}_3$ mode, with $\omega_0 = 4.3$ meV [24] is coupled to the active orbital associated with the half-filled band. In this equation, the creation, $\hat{c}_{i\sigma}^+$, and the annihilation, $\hat{c}_{i\sigma}$, operators, as well as $\hat{n}_{i\sigma} = \hat{c}_{i\sigma}^+ \hat{c}_{i\sigma}$, are fermion operators associated with the i-bonding orbital of the half-filled band, characterized by the hopping interactions T_{ij}, while $\hat{b}_i^+$ and $\hat{b}_i$ are the boson operators associated with the $\bar{u}_3$ phonon.

In this second quantization formalism, the normal mode displacement η_i is given by

$$\sqrt{\frac{1}{(2M\omega_0)}}(\hat{b}_i^+ + \hat{b}_i),$$

(with $\hbar = 1$), $M = 172m_p$ being the effective mass of the $\vec{u}_3$ phonon mode [34,35]; on the other hand, the electronic level associated with the i-bonding orbital is shifted by the phonon mode η_i as follows,

$$\delta E_i = \frac{\partial E_i}{\partial \eta_i}\eta_i = \frac{\partial E}{\partial \eta}\sqrt{\frac{1}{(2M\omega_0)}}(\hat{b}_i^+ + \hat{b}_i),$$

assuming $\partial E_i/\partial \eta_i$ site independent. This equation shows that

$$g = \frac{\partial E}{\partial \eta}\sqrt{\frac{1}{(2M\omega_0)}}; \qquad (2)$$

we calculate $\partial E/\partial \eta$ and g, starting from the (3×3) ground state of the system, and introducing a small displacement $\delta\eta$ for all the Sn atoms (in the 3×3 unit cell), following the $\vec{u}_3$ phonon mode. Using DFT techniques, we calculate $\partial E_0/\partial(\Delta Z)$, E_0 being the energy shift between the up and down surface bands, and ΔZ the vertical distance between up and down Sn atoms. Since the down atoms associated with the metallic band move $1/3$ of the total displacement between up and down Sn atoms, we take $\delta E = \frac{1}{3}\delta E_0$; moreover, the shift in the vertical distance, $\delta(\Delta Z)$, between up and down Sn atoms is given by $\delta(\Delta Z) = \sqrt{\frac{3}{2}}\delta\eta$; these equations show that $\frac{\partial E}{\partial \eta} = \frac{1}{\sqrt{6}}\frac{\partial E_0}{\partial(\Delta Z)}$. Our calculations yield $\frac{\delta E_0}{\delta(\Delta Z)} = 0.85\,\text{eV/Å}$ and $g = 16.8\,\text{meV}$.

It is interesting to realize that this value of $\frac{\partial E_0}{\partial Z}$ is close to, but a little larger than, the one calculated taking ΔE_0 and ΔZ from the difference between the $\sqrt{3} \times \sqrt{3}$ and 3×3 structures: In our calculations [see Figs. 1(d) and S1 in SM] $\Delta E_0 = 0.20\,\text{eV}$ and $\Delta Z_0 = 0.29\,\text{Å}$, so that $\frac{\Delta E_0}{\Delta Z_0} = 0.69\,\text{eV/Å}$; in the calculations of Ref. [20], $\frac{\Delta E_0}{\Delta Z} = 0.73\,\text{eV/Å}$.

The e-ph interaction can be described by means of an e-ph self-energy $\Sigma(\omega)$ [35] in such a way that $m^*/m_0 = 1 - d\Sigma(\omega = 0)/d\omega$, with $d\Sigma(\omega = 0)/d\omega = -\lambda$. We first obtain $\Sigma_{ii}(\omega) \approx \Sigma(\omega)$ for small ω using second-order perturbation theory in the e-ph interaction g, and neglecting the off-diagonal self-energies contributions, $\Sigma_{ij}(\omega) \approx 0$ for $i \neq j$. This approach yields [21]

$$\Sigma^{(2)}(\omega) = -2g^2\rho_0\omega/\omega_0 \quad (\omega \ll \omega_0), \qquad (3)$$

where ρ_0 is the spin local density of states associated with the half-filled electron band. Then, the e-ph mass enhancement parameter $\lambda = -d\Sigma(\omega \to 0)/d\omega$, in second-order perturbation theory, is given by $\lambda^{(2)} = 2g^2\rho_0/\omega_0$.

The spin local density of states ρ_0 is obtained using the experimental evidence of Fig. 2(c), where the bare two-dimensional surface band shows a parabolic behavior below E_F; this two-dimensional band yields a constant density of states, so that $\rho_0 \approx 2.5\,\text{eV}^{-1}$ because there are 0.5 electrons per spin in a bandwidth of 0.2 eV. Then, with $g = 16.8\,\text{meV}$ and $\omega_0 = 4.3\,\text{meV}$, $\lambda^{(2)} \approx 0.32$; this value is quite small as compared to the experimental evidence shown above, $\lambda =$
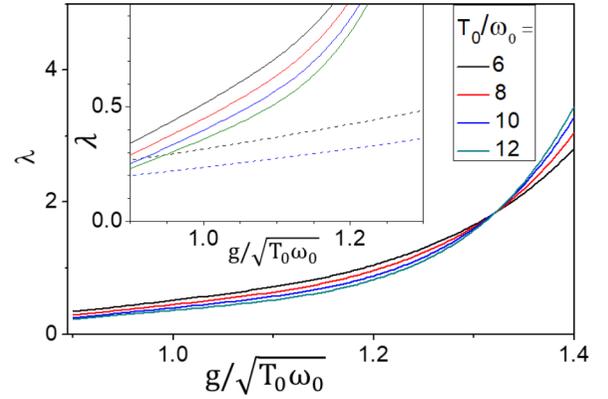
FIG. 3. $\lambda = -d\Sigma_{ii\sigma}(\omega \to 0)/d\omega$ as a function of $g/\sqrt{\omega_0 T_0}$ for the cluster model (see text) for different values of T_0/ω_0. The inset shows λ in a different scale; the dotted lines correspond to $\lambda^{(2)}$ for $T_0/\omega_0 = 6$ and 10.

1.45 ± 0.1, suggesting that contributions beyond the second-order perturbation theory are very important.

In order to go beyond second-order perturbation theory in the electron-phonon interaction g, we follow Refs. [33,36,37] where the half-filled Holstein Hamiltonian of Eq. (1) has been analyzed as a function of g for some particular values of ω_0 and ρ_0. In these works, the lattice model of Eq. (1) is mapped into an associated impurity level that is embedded in a lattice by means of a dynamical mean-field theory numerical renormalization group (DMFT-NRG) calculation. Of particular interest for our case is the calculation in those references, as a function of g, of the quasiparticle weight $Z = [1 - d\Sigma(\omega = 0)/d\omega]^{-1}$ associated with the impurity density of states at the Fermi level ($\omega = 0$); this quantity provides $\lambda = -d\Sigma(\omega = 0)/d\omega = (1 - Z)/Z$, which is shown in Fig. S2 in the Supplemental Material as a function of $g(\rho_0/\omega_0)^{1/2}$. Notice that in is this representation we have changed the abscissa from g to $g(\rho_0/\omega_0)^{1/2}$ because in the limit of small g it is found that

$$\lambda^{(2)} = -d\Sigma^{(2)}(\omega = 0)/d\omega = 2[g(\rho_0/\omega_0)^{1/2}]^2;$$

in this way, for small g, $\lambda^{(2)}$ shows a universal behavior as a function of $g(\rho_0/\omega_0)^{1/2}$. Moreover, plotting λ as a function of $g(\rho_0/\omega_0)^{1/2}$ for the particular values of ρ_0 and ω_0 discussed in the DMFT-NRG calculations [33,36,37] shows a similar behavior (see Fig. S2 in the SM), suggesting that to a good approximation in the DMFT-NRG solution of the half-filled Holstein Hamiltonian λ is a universal function of $g(\rho_0/\omega_0)^{1/2}$.

As an independent check to this conjecture, we have analyzed the case of an impurity embedded in a semi-infinite one-dimensional spinless chain with nearest-neighbor hopping elements T_0 and a local e-ph interaction in the last site of the chain: in this model we neglect the possible off-diagonal self-energy terms between different sites, $\Sigma_{ij}(\omega) = 0$, $i \neq j$, appearing in the lattice of our initial system. Solving numerically this semi-infinite one-dimensional model with the e-ph interaction localized in the impurity is, however, a formidable task in the strong-coupling regime, so that in our analysis we have calculated λ for a cluster of six sites [21].

A general view of our results is presented in Fig. 3, where λ and $\lambda^{(2)}$ are shown as a function of $g/\sqrt{\omega_0 T_0}$ for $T_0/\omega_0 = 6, 8,$ 10, and 12. These results show that $\lambda/\lambda^{(2)} \approx 1$ for $g/\sqrt{\omega_0 T_0} <$ 0.6, while $\lambda/\lambda^{(2)}$ increases steeply for $g/\sqrt{\omega_0 T_0} > 1.0$. In particular, taking $g = 16.8$ meV and $\omega_0 = 4.3$ meV, from our previous calculations, and choosing $T_0/\omega_0 = 9.7$, a value of $g/\sqrt{\omega_0 T_0} = 1.24$ is obtained; this leads to $\lambda^{(2)} = 0.32$, as calculated above in the second-order result, and to $\lambda \approx 1.1$ to all orders in g. Thus, this simple model shows a very important increase in the value of λ, much closer to the experimental result, due to the high-order contributions of g. This increase in λ is also accompanied by an important increase in the average number of phonons in the ground state of our system, $\langle n_{\text{ph}} \rangle \approx 3.5$, this number indicating that there is a large fluctuation of the phonon mode as corresponds to a strong electron-phonon interaction. We should say that this simple model has been used to check the validity of the universal behavior of λ as a function of $g(\rho_0/\omega_0)^{1/2}$; trying to calculate $\Sigma(\omega)$ for $\omega \gtrsim \omega_0$ is beyond the scope of this simple case.

Moreover, Fig. 3 also shows that $g/\sqrt{\omega_0 T_0}$ is a convenient parameter for representing λ and $\lambda^{(2)}$ as a function of the e-ph interaction g, because for the different values of T_0/ω_0, λ presents a very similar behavior, indicating that up to a reasonable approximation λ is a universal function of $g/\sqrt{\omega_0 T_0}$; notice that in the limit of the semi-infinite chain, the curves shown in Fig. 3 should converge, for small g, to the function $\lambda = 2(g\sqrt{\rho_0/\omega_0})^2$ with ρ_0 substituting for $1/T_0$; these arguments indicate that for the semi-infinite chain, with ρ_0 proportional to $1/T_0$, λ is close to a universal function of $g\sqrt{\rho_0/\omega_0}$, at least for $\lambda < 3.0$, confirming the validity of the conjecture deduced from the DMFT-NRG calculations.

Then, for calculating λ for Sn/Ge(111)-(3 × 3), we come back to those DMFT-NRG calculations and take for the Holstein Hamiltonian $\rho_0 = 2.5$ eV^{-1}, $\omega_0 = 4.3$ meV, and $g = 16.8$ meV. These values yield $g\sqrt{\rho_0/\omega_0} = 0.40$ and $\lambda = 1.30 \pm 0.08$ (see SM), in good agreement with the results obtained from the PES experiments. We should mention that the Sn/Ge(111) surface shows an important high-order contribution of the e-ph interaction because of the small frequency ω_0 and the high density of states ρ_0.

V. DISCUSSION AND CONCLUSIONS

We have found from experimental evidence that $\lambda = 1.45 \pm 0.1$, a value much larger than the ones found for Si(111)-(7 × 7) [16], and Ge-Si(111)-(5 × 5) [17]; combining this result with our theoretical value, $\lambda = 1.30$, yields $\lambda = 1.37 \pm 0.10$ which we consider to be a fair approximation to the value of λ for the α-Sn/Ge(111)-(3 × 3) surface.

Regarding our theoretical calculation of the e-ph interaction, it is worth stressing that the interaction has been analyzed by going beyond the second-order term in the g-coupling parameter. Notice also that in our calculations for the α-Sn/Ge(111) surface, $g\sqrt{\rho_0/\omega_0} = 0.40$, and that the second-order calculation in g is only valid for $g\sqrt{\rho_0/\omega_0} < 0.25$ [33]. This suggests that the α-Sn/Ge(111) surface is highly nonlinear in the e-ph coupling, with $\langle n_{\text{ph}} \rangle \approx 3.5$, and that the usual way of defining the quasiadiabatic effective phonon-induced

attraction, measured by $U_{\text{negative}} = 2g^2/\omega_0$ [36], should be reconsidered.

At this point we argue as follows: Our calculations from the second-order approximation yield that $U_{\text{negative}} = 2g^2/\omega_0 = \lambda^{(2)}/\rho_0$. Then, we suggest that, in order to include the higher-order contributions, it seems convenient to define a renormalized $U_{\text{negative}} = \lambda/\rho_0$ which extrapolates the second-order limit to higher values of g.

It is worth considering now the value of U_{negative}, as deduced from the value of $\lambda = 1.37 \pm 0.1$. This yields $U_{\text{negative}} = \lambda/\rho_0 = 0.55 \pm 0.06$ eV, with this quantity being close to, but slightly larger than, the value calculated for the effective e-e interaction for the α-Sn/Ge(111)-(3 × 3) surface, $(U - V) \approx 0.43$ eV [4]. From these figures we conclude that the low-temperature phases of α-Sn/Ge(111), including a possible superconducting state, should appear as a result of a delicate balance between the e-ph and e-e interactions.

VI. METHODS

Photoemission experiments were performed at the high-resolution branch of CASSIOPEE beamline at Soleil synchrotron. The ultrahigh vacuum setup couples a surface preparation chamber equipped with LEED and a high-resolution ARPES chamber equipped with a manipulator operating between 400 and 5 K and with a Scienta R4000 electron analyzer having a $\pm 15°$ acceptance angle. Incoming radiation and the normal to the detector center subtend a $45°$ angle. In our experiments, we settled the light polarization in the plane defined by these two directions while the detector slit was perpendicular to them. The valence band measurements were performed at $h\nu = 80$ eV. The sample preparation has been described elsewhere [4]. The 0.33-ML Sn surface coverage was calibrated from the Sn 4d/Ge 3d intensity ratio, surface state intensity, and the evolution of the LEED pattern.

In the DFT calculations we have used the QUANTUM ESPRESSO code [38] with the Perdew-Burke-Ernzerhof (PBE) exchange-correlation functional [39] and the ultrasoft pseudopotentials provided by the code. The (3 × 3) surface slab was built with 11 Ge layers and 3 Sn adatoms in T_4 positions in the upper layer. The dangling bonds of the lowest Ge layer are saturated by H atoms. The lower two Ge layers and the H atoms are fixed in the simulations. See Supplemental Material [21] for more details (see also Refs. [38–40] therein).

[1] P. C. Snijders and H. H. Weitering, Rev. Mod. Phys. **82**, 307 (2010).

[2] X. Wu, F. Ming, T. S. Smith, G. Liu, F. Ye, K. Wang, S. Johnston, and H. H. Weitering, Phys. Rev. Lett. **125**, 117001 (2020).

[3] N. J. DiNardo, T. M. Wong, and E. W. Plummer, Phys. Rev. Lett. **65**, 2177 (1990).

[4] R. Cortés, A. Tejeda, J. Lobo-Checa, C. Didiot, B. Kierren, D. Malterre, J. Merino, F. Flores, E. G. Michel, and A. Mascaraque, Phys. Rev. B **88**, 125113 (2013).

[5] R. Cortés, A. Tejeda, J. Lobo, C. Didiot, B. Kierren, D. Malterre, E. G. Michel, and A. Mascaraque, Phys. Rev. Lett. **96**, 126103 (2006).

[6] J. M. Carpinelli, H. H. Weitering, M. Bartkowiak, R. Stumpf, and E. W. Plummer, Phys. Rev. Lett. **79**, 2859 (1997).

[7] J. Avila, A. Mascaraque, E. G. Michel, M. C. Asensio, G. LeLay, J. Ortega, R. Pérez, and F. Flores, Phys. Rev. Lett. **82**, 442 (1999).

[8] B. Guster, R. Robles, M. Pruneda, E. Canadell, and P. Ordejón, 2D Mater. **6**, 015027 (2019).

[9] T. Aruga, Surf. Sci. Rep. **61**, 283 (2006).

[10] J. M. Kosterlitz and D. J. Thouless, J. Phys. C **6**, 1181 (1973).

[11] B. I. Halperin and D. R. Nelson, Phys. Rev. Lett. **41**, 519(E) (1978).

[12] T. S. Smith, F. Ming, D. G. Trabada, C. González, D. Soler-Polo, F. Flores, J. Ortega, and H. H. Weitering, Phys. Rev. Lett. **124**, 097602 (2020).

[13] G. Li, P. Höpfner, J. Schäfer, C. Blumenstein, S. Meyer, A. Bostwick, E. Rotenberg, R. Claessen, and W. Hanke, Nat. Commun. **4**, 1620 (2013).

[14] D. G. Trabada, J. I. Mendieta-Moreno, D. Soler-Polo, F. Flores, and J. Ortega, Appl. Surf. Sci. **479**, 260 (2019).

[15] S. Wolf, D. Di Sante, T. Schwemmer, R. Thomale, and S. Rachel, Phys. Rev. Lett. **128**, 167002 (2022).

[16] I. Barke, F. Zheng, A. R. Konicek, R. C. Hatch, and F. J. Himpsel, Phys. Rev. Lett. **96**, 216801 (2006).

[17] M. Stoffel, Y. Fagot-Revurat, A. Tejeda, B. Kierren, A. Nicolaou, P. Le Fèvre, F. Bertran, A. Taleb-Ibrahimi, and D. Malterre, Phys. Rev. B **86**, 195438 (2012).

[18] G. Anemone, M. Garnica, M. Zappia, P. C. Aguilar, A. Al Taleb, C.-N. Kuo, C. S. Lue, A. Politano, G. Benedek, and A. L. V. de Parga, 2D Mater. **7**, 025007 (2020).

[19] N. F. Hinsche and K. S. Thygesen, 2D Mater. **5**, 015009 (2018).

[20] O. Pulci, M. Marsili, P. Gori, M. Palummo, R. Del Sole, A. Cricenti, F. Bechstedt, Appl. Phys. A **85**, 361 (2006).

[21] See Supplemental Material at http://link.aps.org/supplemental/10.1103/PhysRevB.107.045303 for details of the DFT calculations, a discussion of the band narrowing due to the *e-e* interaction, details of the second-order perturbation theory, and details of the cluster calculation.

[22] A. C. Hewson, *The Kondo Problem to Heavy Fermions* (Cambridge University Press, Cambridge, UK, 1993).

[23] B. Horvatié and V. Zlatic, J. Phys. France **46**, 1459 (1985).

[24] D. Farías, W. Kamiński, J. Lobo, J. Ortega, E. Hulpke, R. Pérez, F. Flores, and E. G. Michel, Phys. Rev. Lett. **91**, 016103 (2003).

[25] R. Pérez, J. Ortega, and F. Flores, Phys. Rev. Lett. **86**, 4891 (2001).

[26] S. de Gironcoli, S. Scandolo, G. Ballabio, G. Santoro, and E. Tossatti, Surf. Sci. **454**, 172 (2000).

[27] J. A. Sobota, Y. He, and Z. X. Shen, Rev. Mod. Phys. **93**, 025006 (2021).

[28] M. Hengsberger, D. Purdie, P. Segovia, M. Garnier, and Y. Baer, Phys. Rev. Lett. **83**, 592 (1999).

[29] A. Lanzara, P. V. Bogdanov, X. J. Zhou, S. A. Kellar, D. L. Feng, E. D. Lu, T. Yoshida, H. Eisaki, A. Fujimori, K. Kishio, J.-I. Shimoyama, T. Nodak, S. Uchidak, Z. Hussain, and Z.-X. Shen, Nature (London) **412**, 510 (2001).

[30] E. W. Plummer, J. Shi, S.-J. Tang, Eli Rotenberg, and S. D. Kevan, Prog. Surf. Sci. **74**, 251 (2003).

[31] M. Mulazzi, G. Rossi, J. Braun, J. Minar, H. Ebert, G. Panaccione, I. Vobornik, and J. Fujii, Phys. Rev. B **79**, 165421 (2009).

[32] G. Benedek, J. R. Manson, and S. Miret-Artés, Phys. Chem. Chem. Phys. **23**, 7575 (2021).

[33] D. Meyer, A. C. Hewson, and R. Bulla, Phys. Rev. Lett. **89**, 196401 (2002).

[34] J. M. Ziman, *Electrons and Phonons* (Oxford University Press, Oxford, UK, 1960).

[35] G. D. Mahan, *Many-Particle Physics* (Springer, Berlin, 2000).

[36] W. Koller, D. Meyer, and A. C. Hewson, Phys. Rev. B **70**, 155103 (2004).

[37] A. C. Hewson and D. Meyer, J. Phys.: Condens. Matter **14**, 427 (2002).

[38] A. Dal Corso, Comput. Mater. Sci. **95**, 337 (2014).

[39] J. P. Perdew, K. Burke, and M. Ernzerhof, Phys. Rev. Lett. **77**, 3865 (1996).

[40] M. J. Monkhorst and J. D. Pack, Phys. Rev. B **13**, 5188 (1976).